J. Phys. Earth, **32**, 317–338, 1984

ANALYTICAL AND SEMI-EMPIRICAL SYNTHESIS OF NEAR-FIELD SEISMIC WAVEFORMS FOR INVESTIGATING THE RUPTURE MECHANISM OF MAJOR EARTHQUAKES

Kazuhiko IMAGAWA, Naoya MIKAMI,* and Takeshi MIKUMO

Disaster Prevention Research Institute, Kyoto University, Uji, Kyoto, Japan

(Received June 1, 1984; Revised August 11, 1984)

For predicting strong ground motions from major earthquakes and for close investigations into complex rupture processes, two different analytical and semi-empirical approaches are used to synthesize seismic waves from a nearby fault with a large linear dimension. The former technique is to calculate Green's functions for a horizontally layered structure by the discrete wavenumber/finite element method, and the latter is to use the records of minor shocks as empirical Green's functions by convolving a correction function for the differences in the source functions and the receiver responses between the main and smaller events. In both cases, the phase-delayed Green's functions are integrated over the entire fault surface.

The above methods have been applied to the case of the 1969 central Gifu earthquake (M=6.6) which was followed by moderate aftershocks (M=4.3–4.8) and a number of smaller events. It was found that the waveforms synthesized from the two approaches agree reasonably well with each other. The strong-motion records, particularly of body waves and the major portion of surface waves with periods longer than 5–7 s, can be satisfactorily modeled by the theoretical synthesis with a realistic structure and also by the semi-empirical analysis using four aftershock records, if reasonable rupture velocities and rise times are assumed.

However, the shorter-period waves with periods 1–2 s involved in the records cannot be simulated by either of these syntheses, unless incoherent rupture propagation over the fault is included. A stochastic fault model with variable rupture velocities over large-scale fault segments is tentatively presented to account for the short-period waves.

1. *Introduction*

Seismic waveforms observed in the near-field during major earthquakes depend primarily on complex dynamic rupture processes on the fault, but also on

* Present address: Meteorological Research Institute, Japan Meteorological Agency, Tsukuba, Ibaraki, Japan

heterogeneous crustal structures around the source, and propagation and recording site effects. For the purpose of predicting strong motions from a large earthquake, all these effects should be fully taken into consideration. In order to investigate the complex faulting process from strong motion records, on the other hand, the effects of wave propagation through a heterogeneous earth must first be understood.

A number of theoretical studies have so far been developed to predict seismic waveforms and to simulate the observed seismograms of strong ground motions in the near-field. The earlier and most fundamental work (AKI, 1968; HASKELL, 1969) uses simple dislocation sources in an infinite homogeneous medium (MARUYAMA, 1963; BURRIDGE and KNOPOFF, 1964), and later on double-couple point sources in a half-space (e.g., KAWASAKI *et al.*, 1973, 1975), incorporating the free surface effect. It has been found that these simple models are useful for simulating mainly long-period direct body waves, and also converted body and Rayleigh waves in the latter case. Observed seismograms, however, usually reflect propagation through a more complicated structure, including high-frequency seismic waves refracted and reflected at many small-scale geological boundaries in the real earth's structure. Theoretical approaches have since been advanced to incorporate the seismic wave response of more realistic, horizontally layered crustal structures. The response of the medium due to a double-couple point source, or Green's function, has been calculated by various analytical techniques: generalized ray theory (e.g., HELMBERGER, 1968; HELMBERGER and MALONE, 1975; HEATON and HELMBERGER, 1977, 1978), Cagniard-deHoop method for a series of multiply-reflected rays (SATO, 1977, 1978), reflectivity methods (FUCHS and MÜLLER, 1971; KENNETT, 1974; KENNETT and KERRY, 1979), direct frequency-domain integration (HERRMANN and NUTTLI, 1975a, b; HERRMANN, 1977; WIGGINS *et al.*, 1977), normal mode method (e.g., KAWASAKI, 1978; SWANGER and BOORE, 1978), discrete wave-number method (BOUCHON, 1979, 1981), reflectivity method together with the Cagniard-deHoop integration (SATO and HIRATA, 1980), and by the discrete wave-number/finite element method (ALEKSEEV and MIKHAILENKO, 1980; HRON and MIKHAILENKO, 1981; OLSON, 1982). The last may be the most comprehensive method to generate the complete response of a vertically heterogeneous medium, including all types of body and surface waves. Practical examples of numerical calculations based on this method will be presented in later sections.

However, the real earth's structure travelled by seismic waves may be much more complicated than assumed above, which includes lateral heterogeneities, attenuative properties, and even local topographical site effects, and hence their complete modeling would be extremely difficult. To overcome this difficulty, a semi-empirical approach has been presented by HARTZELL (1978) to model strong ground motions from a large earthquake using its aftershock records as an empirical earth's response. This is based on the idea that if the source of a minor shock, such as a foreshock or aftershock, is small enough to be approximated as a point

source on the main shock fault, the ground motion associated with the small event may be regarded as a Green's function which involves all the propagating effects from the source to receiver. This technique first applied to the 1940 Imperial Valley earthquake has proved effective to simulate long-period components ($T>$ 8 s) of the main-shock seismograms (HARTZELL, 1978). Similar approaches have been employed to predict the velocity spectra, peak accelerations, and the maximum duration of ground motions from large earthquakes with complex multiple events (KANAMORI, 1979; HADLEY and HELMBERGER, 1980). IRIKURA and MURAMATU (1982), IMAGAWA and MIKUMO (1982), and IRIKURA (1983) have extended Hartzell's method by convolving the phase delayed records with a specific time function to correct for the difference in the source time function and other fault parameters between the main shock and smaller events.

In all these cases, however, the small shocks should have the same focal mechanism as the main shock event and should also be large enough to excite the response sufficiently above the noise level (HARTZELL, 1978). Besides these limitations, it is essential that these small events with appropriate sizes be distributed over the entire fault of the main shock, for the synthesis of ground motions for the main event. This is required since the Green's function depends on the location on the fault surface and on the recording site, and hence its form differs considerably from place to place.

The final goal of our studies is to infer dynamic faulting processes of major earthquakes using strong motion records, which may be characterized by incoherent rupture propagation, non-uniform slip displacements, complex source time functions, etc. As a first step toward this goal, we attempt in the present paper to synthesize ground motions from a moderate earthquake by applying both of the analytical and semi-empirical techniques described above. The utility of the two methods in modeling the actual ground motions are carefully compared, and their applicability to further investigations into more complex faulting processes are discussed. As a next step in this study, we tentatively introduce a stochastic fault model with variable rupture velocities to provide a possible explanation for the high-frequency waves which are seen in the observed seismograms but could not be explained by a simple, uniform rupture.

2. *Methods for Theoretical and Semi-Empirical Synthesis of Ground Motions*

The methods we used here for the synthesis of ground motions from a main shock are essentially based on the representation theorem for a kinematic dislocation model in an elastic medium. The displacement field due to a slip dislocation over a fault S can be expressed by (e.g., BURRIDGE and KNOPOFF, 1964)

$$\boldsymbol{u}^i(\boldsymbol{y}, t)=\int_0^t \mathrm{d}\tau \iint_S \boldsymbol{S}(\boldsymbol{x}, \tau)\cdot \boldsymbol{g}^i(\boldsymbol{x}, t-\tau, \boldsymbol{y})\, \mathrm{d}S, \tag{1}$$

where $\boldsymbol{u}^i(\boldsymbol{y}, t)$ is the i-th component of displacement at a location $\boldsymbol{y}$ and time t,

$S(x, t)$ is the slip discontinuity across the fault surface at a position x at $t=\tau$, and $g^i(x, t-\tau, y)$ is the stress tensor at position x and time t due to an impulsive point force applied in the i-th direction at the location y. $g^i(x, t-\tau, y)$ may also be taken as the i-th component of displacement at the receiver position y due to a point dislocation at x on the fault, and hence may be regarded as the Green's function or the impulse response of the medium. Equation (1) thus implies that the displacement at any point in the medium is expressed by the convolution of the slip distribution with the Green's function, integrated over the fault surface. When the direction of the displacement discontinuity is the same everywhere on the fault surface, the slip can be written as $S(x, t)=m^i \Delta u(x, t)$, where m^i is the second-order moment tensor for a point shear dislocation, which is specified by the direction of the fault plane, and $\Delta u(x, t)$ is the scalar slip or source function. If we further assume that the position x on the fault plane starts to slip at time t' specified by the rupture propagation, t can be replaced by $t-t'$, and Eq. (1) may also be expressed by

$$u^i(y, t)=\int_0^{t-t'} d\tau \iint_S m^i \Delta u(t-t'-\tau) \cdot g^i(x, \tau, y)\, dS. \tag{2}$$

2.1 Theoretical synthesis

To perform the integration (2) over the fault, we divide the entire fault surface with dimension $S=L \times W$ into N segments each of which has an elementary size of $\Delta S_j=L_j \times W_j$, as shown in Fig. 1. The displacement as given by Eq. (2) may be rewritten as,

$$\begin{aligned} u^i(t) &= \sum_{j=1}^{N} m_j^i \Delta u(t-t_j) * g_j^i(t) \Delta S_j \\ &= \sum_{j=1}^{N} m_j^i \Delta u(t) * g_j^i(t-t_j) \Delta S_j, \end{aligned} \tag{3}$$

where the subscript j refers to the j-th fault segment, the symbol $*$ indicates a con-

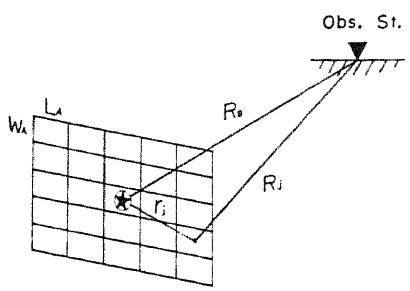

Fig. 1. Geometry of the fault plane and an observation station. Symbol ✱ indicates the location of hypocenter. R_0 and R_j are the distances from the initiation point of rupture and from the j-th fault segment to the station, and r_j is the distance between the two points on the fault.

volution operator, and t_j is the phase delay time from the onset of initial rupture. t_j is expressed by $t_j=r_j/v+(R_j-R_0)/c$ (See Fig. 1), v and c being the rupture velocity over the fault and the average wave velocity in the medium, respectively. If the distance R_j along the ray path between each of the divided segments ΔS_j and the receiver position y is much greater than the linear dimension of the segments, i.e., $\lambda R/2 \gg L_j^2$ (e.g., AKI and RICHARDS, 1980, Chap. 8 equation (14. 12)), the far-field terms involved in the Greens' function dominate over the other terms, and the displacement $u^i(y, t)$ should have a waveform proportional to

$$\iint_S \Delta\dot{u}\,(x,\ t-t')\ \mathrm{d}S.$$

In this case, $\Delta u(t)$ in Eq. (3) may be replaced by $\Delta\dot{u}(t)$, and $g_j^i(t)$ reduces to the Green's function only for the far-field.

We assume here that the slip function $\Delta u(t)$ has the following ramp functional form,

$$\begin{aligned} \Delta u(t) &= (Dt/\tau)H(t) \quad (t<\tau) \\ &= D \qquad\qquad\ (t\geqq\tau), \end{aligned} \tag{4}$$

where D is the final displacement, τ is the rise time, and $H(t)$ is the Heaviside unit step function. The synthetic seismogram can be obtained by convolving $u_j^i(t)$ with the impluse response $h(t)$ of the seismograph used,

$$f^i(t)=u^i(t)*h(t). \tag{5}$$

In order to calculate the Green's function $g_j^i(t)$, we use the discrete wave-number/finite element method (abbreviated as the DWFE method) presented recently by OLSON (1982), which is similar to that given by ALEKSEEV and MIKHAILENKO (1980). The DWFE method yields the complete elastic response of a vertically heterogeneous medium, by combining separable solutions of the elastic equations for the horizontal dependence of the wave motion in terms of a Fourier-Bessel series, with finite element and finite difference solutions for the vertical and time dependence (OLSON, 1982). For numerical calculations, we used a computer program originally written by A. Olson, and somewhat modified for our purpose. $g_j^i(t)$ obtained from this method includes all types of body and surface waves, and also near-field terms. The Green's functions are then convolved with the slip function multiplied by the second order moment tensor and spatially integrated over the fault surface to obtain the theoretical displacements, as given by Eq. (3).

2.2 Semi-empirical synthesis

Suppose we use the records of small events, such as from foreshocks and aftershocks, as empirical Green's functions, instead of calculating the theoretical functions. If the source of the small event can be approximated as a point source located in the far-field, and if the source duration is short enough, then $\Delta(\dot{u})t\rightarrow$

$\delta(t)$, and the observed seismogram reduces to, $f_A(t) \propto m_j^i g_j^i(t) * h(t)$, which includes only the propagation effects and the instrumental response. This is not always the case, however. If, instead, we utilize the observed seismogram from a minor event with a small but finite source area and a finite rise time,

$$f_{Aj}^i(t) = m_{Aj}^i \Delta\dot{u} \Delta\dot{u}_{Aj}(t) * g_j^i(t) \Delta S_{Aj} * h_A(t), \tag{6}$$

where the subscript A denotes the quantities belonging to the minor event that occurred at the j'th location. The fault area of the main shock is then divided into a finite number of segments with a unit dimension equal to the source area of the small events, i.e., $L_j = L_A$, $W_j = W_A$. The main-shock seismogram may be synthesized from a modified form of Eqs. (3) and (5).

$$f_M^i(t) = h_M(t) * \sum_{j=1}^{N} m_j^i \Delta\dot{u}_{Mj}(t) * g_j^i(t - t_j) \Delta S_j. \tag{7}$$

Taking the Fourier transform of Eqs. (6) and (7), we have

$$\begin{aligned} F_M^i(\omega) &= H_M(\omega) \sum_{j=1}^{N} m_j^i \Delta\dot{U}_{Mj}(\omega) G_j^i(\omega) e^{-i\omega t_j} \Delta S_j \\ &= \sum_{j=1}^{N} Q_j(\omega) F_{Aj}(\omega) e^{-i\omega t_j} \end{aligned} \tag{8}$$

$$Q_j(\omega) \equiv (\Delta\dot{U}_{Mj}(\omega) / \Delta\dot{U}_{Aj}(\omega))(H_M(\omega) / H_A(\omega)) \tag{9}$$

since $m_j^i G_j^i(\omega) \Delta S_j = m_{Aj}^i G_j^i(\omega) \Delta S_{Aj}$. We assumed here that the waveforms of the main shock and aftershocks were recorded with two different types of instruments with different amplifications and frequency responses but at a single station. From Eq. (8), the synthetic seismogram for the main shock may be given by,

$$f_M^i(t) = \sum_{j=1}^{N} q_j(t) * f_A(t - t_j) \tag{10}$$

where

$$q_j(t) = \int_{-\infty}^{\infty} Q_j(\omega) e^{-i\omega t} \mathrm{d}\omega, \tag{11}$$

(MIKUMO, 1981; IMAGAWA and MIKUMO, 1982).

If the slip displacement and the rise time of the main shock are uniformly distributed over the fault plane, and if we could use aftershocks with identical slips and rise times, $Q_j(\omega)$ and $q_j(t)$ turn out to be constant, and may be replaced by $Q(\omega)$ and $q(t)$. In this case, Eq. (10) can be rewritten as

$$f_M^i(t) = q(t) * \sum_{j=1}^{N} f_A(t - t_j). \tag{12}$$

$q_j(t)$ and $q(t)$ are correction functions for the differences in the source time function between the main shock and smaller events, and also between the instrumental responses used for recording the two different types of shocks.

The ratio $\Delta\dot{U}_M(\omega)/\Delta\dot{U}_A(\omega)$, which is obtained on the basis of Eq. (4), includes the ratios of the final displacement and the rise times for the main shock and the smaller events used. One possible way of estimating these ratios was to use some empirical formulae between the fault parameters and the earthquake magnitude M (IMAGAWA and MIKUMO, 1982). Another way is to rely on scaling relations between the fault parameters, assuming that these relations hold between the main shock and smaller events that occurred on a single fault plane. If we use the empirical similarity conditions proposed by KANAMORI and ANDERSON (1975), the scaling relations may be written as (IRIKURA and MURAMATU, 1982; IRIKURA, 1983),

$$L_M/L_A = W_M/W_A = D_M/D_A = \tau_M/\tau_A = (M_{0M}/M_{0A})^{1/3}. \tag{13}$$

Both of the ratios D_M/D_A and τ_M/τ_A can be obtained from the moment ratio M_{0M}/M_{0A}, which may be estimated from the spectral amplitudes at low frequencies (IRIKURA, 1983) or again from an empirical formula (KANAMORI and ANDERSON, 1975)

$$\log (M_{0M}/M_{0A}) = 1.50\ (M_M - M_A).$$

However, the above scaling relations also assume $D_M/\tau_M = D_A/\tau_A$, which gives the same slip velocity for the larger and smaller events. It has so far been reported for many earthquakes, however, that the slip velocity on the fault surface depends on the local stress drop, and also that the average stress drop estimated for a number of events ranges between 1 and 100 bar. Since this result does not warrant the above assumption, we have tried many different combinations for the rise times.

3. *Observed Data*

In the present paper, the methods described above have been applied to the central Gifu earthquake of September 9, 1969 ($M=6.6$), which was a moderate-size inland earthquake in central Japan. The focal mechanism solution and the spatial distribution of a number of aftershocks indicate that this earthquake was caused by left-lateral strike-slip motion along a vertical fault plane trending in the N30°W direction. The fault parameters of the main shock estimated from the aftershock distribution, strong-motion records, vertical tectonic movements, and some additional data are $L=18$–23 km, $W=10$ km, $D=64$–72 cm, $M_0=3.5$–5.0×10^{25} dyn·cm, $\tau=1.0$–1.5 s, $v=2.0$–2.5 km/s (MIKUMO, 1973).

Seismic waves from this earthquake were well recorded at five JMA stations within epicentral distances less than 80 km with strong-motion seismographs. Among these, three-component strong-motion records at the Gifu station ($\Delta=51$ km) have been selected and are used for the present study. The instrumental constants of the seismographs are natural period of 6 s for the horizontal, and 5 s for the vertical components, respectively, and damping constant of 0.6. Most of the aftershocks are distributed in a belt-like zone extending for about 20 km,

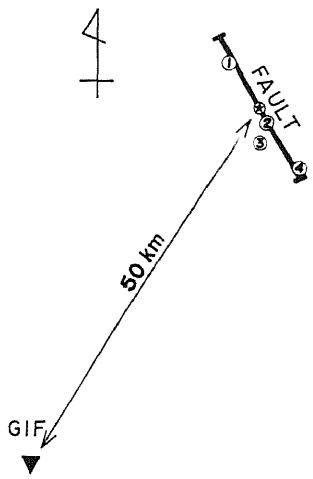

Fig. 2. Map indicating the location of the presumed fault trace for the 1969 central Gifu earthquake and a recording station. Symbol ⊛ indicates the epicenter of the main shock, and numerals indicate the location of the aftershocks used in the present study.

and their focal depths range between 2 and 12 km. Among these aftershocks, we selected four aftershocks with magnitudes 4.3, 4.8, 4.5, and 4.6 that occurred from northwest to southeast along the presumed main shock fault. The aftershocks were recorded by Wiechert-type seismographs (with a magnification 80) the Gifu station. Figure 2 shows the locations of the presumed fault, the main shock, and the four aftershocks used in the present study. The strong-motion records of the main shock and the aftershock records are shown in later sections.

4. *Results from Theoretical Synthesis*

In this section, we calculate, as a first step, theoretical Green's functions using the DWFE method to estimate the effects of crustal layering and source depth by comparing them with the corresponding aftershock records. For the crustal structure appropriate to the profile between the source area and the Gifu station, we tentatively adopt a velocity model (UKAWA and FUKAO, 1982) which has been obtained for the Chubu region, Honshu, Japan, using P and S wave arrival times from crustal and subcrustal earthquakes. The velocity structure, designated Model 1, is given in Table 1 and Fig. 3. The Green's functions calculated for epicentral locations of aftershocks No. 2 and No. 4 and for five different source depths in this structure are shown in Figs. 4 and 5, together with the corresponding aftershock records. Each of the calculated traces includes the seismograph response, and is normalized to have the same maximum amplitude in these figures. The cut-off frequency in this calculation is 1.2 Hz. We assume a point disloca-

Table 1. Crustal models used in the present study.

Model 1

Layer thickness (km)	V_P (km/s)	V_S (km/s)	Density (g/cm^3)
4.0	5.5	3.25	2.65
20.0	6.11	3.61	2.74
10.0	7.15	4.01	3.0
	7.81	4.41	3.22

Model 2

Layer thickness (km)	V_P (km/s)	V_S (km/s)	Density (g/cm^3)
0.66	3.2	2.0	2.3
1.12	4.76	2.58	2.4
2.16	5.5	3.25	2.65
20.0	6.11	3.61	2.74
10.0	7.15	4.01	3.0
	7.81	4.41	3.22

Model 1 is taken from UKAWA and FUKAO (1982).

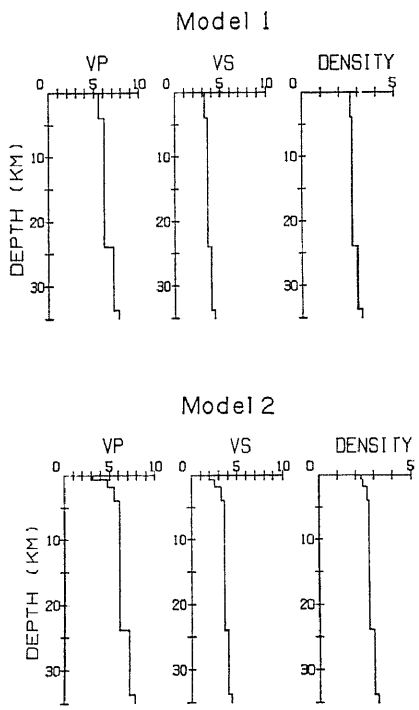

Fig. 3. Two possible crustal models, named Model 1 and Model 2, which are used to compute the theoretical seismograms. V_P, P-wave velocity (in km/s); V_S, S-wave velocity (in km/s); DENSITY, density (in g/cm^3). Model 1 is taken from UKAWA and FUKAO (1982).

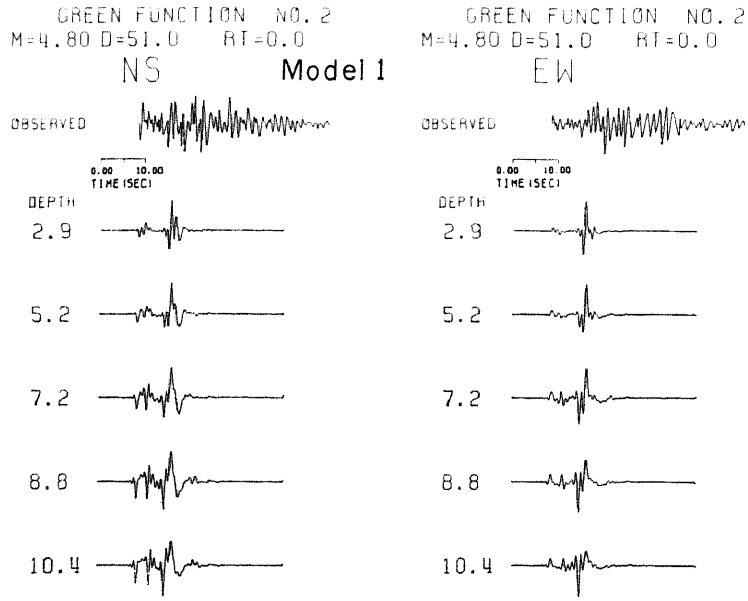

Fig. 4. Observed seismograms of aftershock No. 2 (top traces), and the Green's functions calculated for the corresponding location and several different source depths for Model 1. The source function is assumed to be a step function. Each trace is normalized to have the same maximum amplitude. The same explanations apply to Figs. 5, 6, and 7.

tion source, and a step function (with the rise time $\tau=0$) for the source function. We immediately notice in Figs. 4 and 5 that the calculated traces have much shorter duration than the aftershock records, although they show somewhat similar waveforms to the first half of the records.

We feel that one possible reason for the shorter durations of the Green's functions for Model 1 may be due to the lack of a soft sedimentary layer at the top of the crustal structure. The existence of the sedimentary layer would generate reverberations of seismic waves and hence would make the durations much longer. For this reason, we arbitrarily assume that there could be two surficial low-velocity layers overlying the structure which have not been well identified in the previous P and S travel time study. The modified model, which is called Model 2, is also shown in Table 1 and Fig. 3. Figures 6 and 7 illustrate the Green's functions calculated from Model 2, arranged in the same way as in Figs. 4 and 5. It is noticed that the duration times for these traces are remarkably extended, as compared with those for the corresponding traces from Model 1, particularly for shallower source depths. As may be expected, the later portion of the calculated traces are surface waves excited by reverberations within the low-velocity surface layers. Important features to be also noted here are that the calculated functions vary considerably with source depth for a fixed epicentral distance, and that small dif-

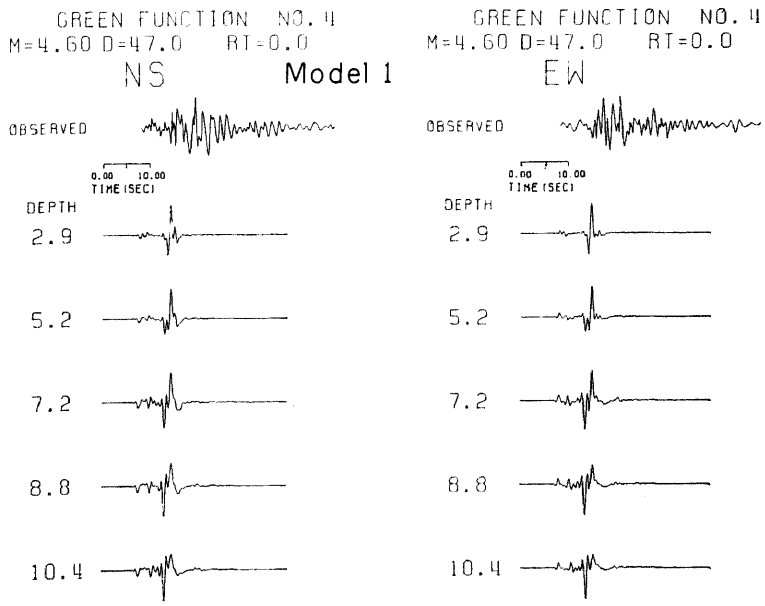

Fig. 5. Observed seismograms of aftershock No. 4 (top traces), and the Green's functions calculated for the corresponding location and several different source depths for Model 1.

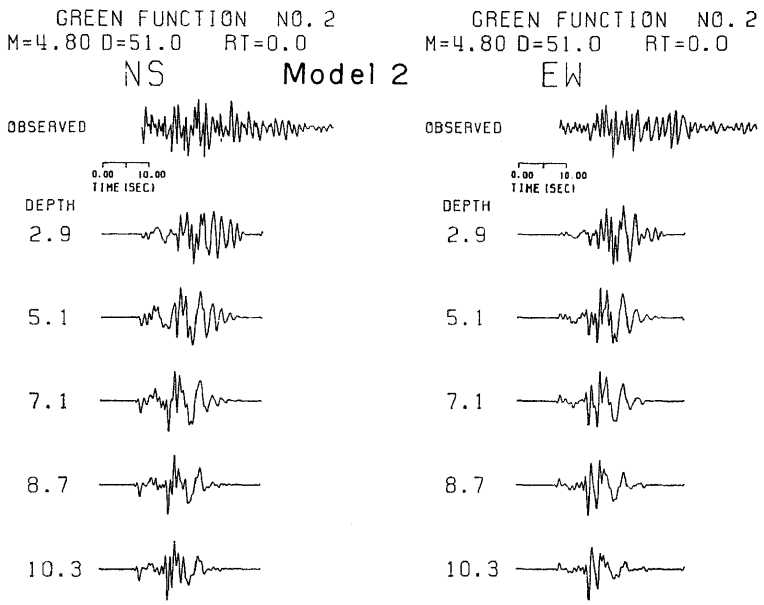

Fig. 6. Observed seismograms of aftershock No. 2 (top traces), and the Green's functions calculated for the corresponding location and several different source depths for Model 2.

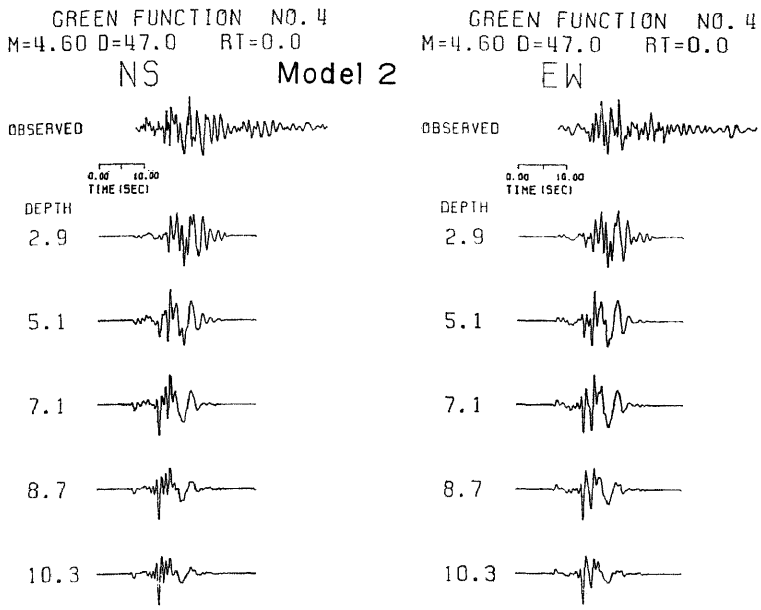

Fig. 7. Observed seismograms of aftershock No. 4 (top traces), and the Green's functions calculated for the corresponding location and several different source depths for Model 2.

ferences in the distance and the azimuth yield appreciable differences in the waveform of the Green's function, as shown in Figs. 6 and 7. If we compare these traces with the aftershock records, we see that the observed seismograms from aftershock No. 4 may be satisfactorily explained for about 20 s by the uppermost traces with a source depth of 2.9 km. However, the agreement between the records for aftershock No. 2 and the calculated traces is not as good as that for No. 4. The reason for this might be due either to small-scale lateral heterogeneities in the actual structure along the propagation paths from aftershocks No. 4 and No. 2 to the recording site, or to a somewhat complicated rupture process in aftershock No. 2. This type of discrepancy and the variations of the calculated Green's functions with source depth present some problems for semi-empirical predictions of strong-motions when using only a small number of records from minor events.

The next step is to synthesize theoretical seismograms for the main shock by using the above Green's functions. For this purpose, the Green's functions calculated for each of the fault segments are integrated over the fault plane, with appropriate phase delay times, and are convolved with the slip function, as given in Eq. (3). The dimension of the fault segments is taken as 2 km$\times$2 km. The fault rupture is assumed to initiate at the center of the fault plane and spread radially at a constant velocity, and the final slip is assumed to be constant over the fault plane. We assume several different rupture velocities, rise times and

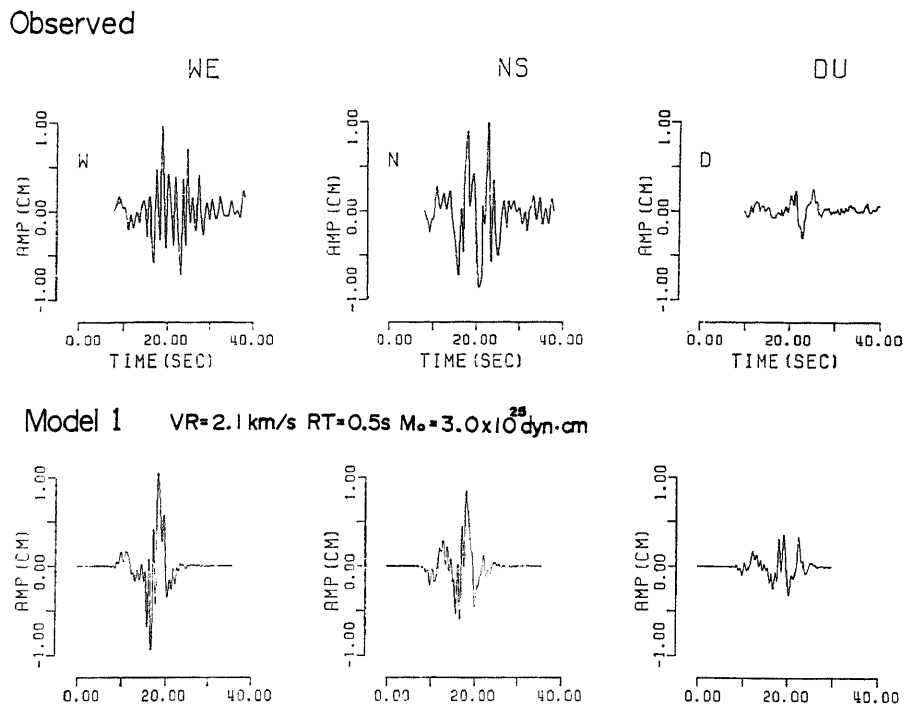

Fig. 8. Strong-motion records from the central Gifu earthquake of September 9, 1969 (M=6.6) at the GIF station, and the corresponding synthetic seismograms computed for Model 1. Rupture velocity VR, rise time RT and seismic moment M_0 are assumed to be 2.1 km/s, 0.5 s, and 3.0×10^{25} dyn·cm, respectively.

seismic moments. Examples of the calculated results for two different cases are shown in Figs. 8 and 9.

Figure 8 gives the synthetic seismograms calculated for one of the possible crustal structures, Model 1, in comparison with the corresponding three-component strong-motion records obtained at the Gifu station. The observed and synthetic seismograms are plotted on the same scale, as indicated in the ordinate. The rupture velocity, rise time, and seismic moment in this case are taken as 2.1 km/s, 0.5 s, and 3.0×10^{25} dyn·cm, respectively. From a close comparison of the corresponding components of the observed and synthetic seismograms, we see that the recorded waveforms over about 10 s from the onset, which include P and S waves, have been reproduced quite well by this synthesis. However, later surface wave portions on the two horizontal components, including a large third peak, cannot be satisfactorily simulated. The synthetic seismograms obtained for Model 2 are shown in Fig. 9, where the rupture velocity is taken as 2.3 km/s and the other two parameters remain the same. We notice that the synthesis from the latter model gives a better fit to the data, not only to the general waveform but also to the large amplitude phase arriving about 15 s after the onset, suggesting

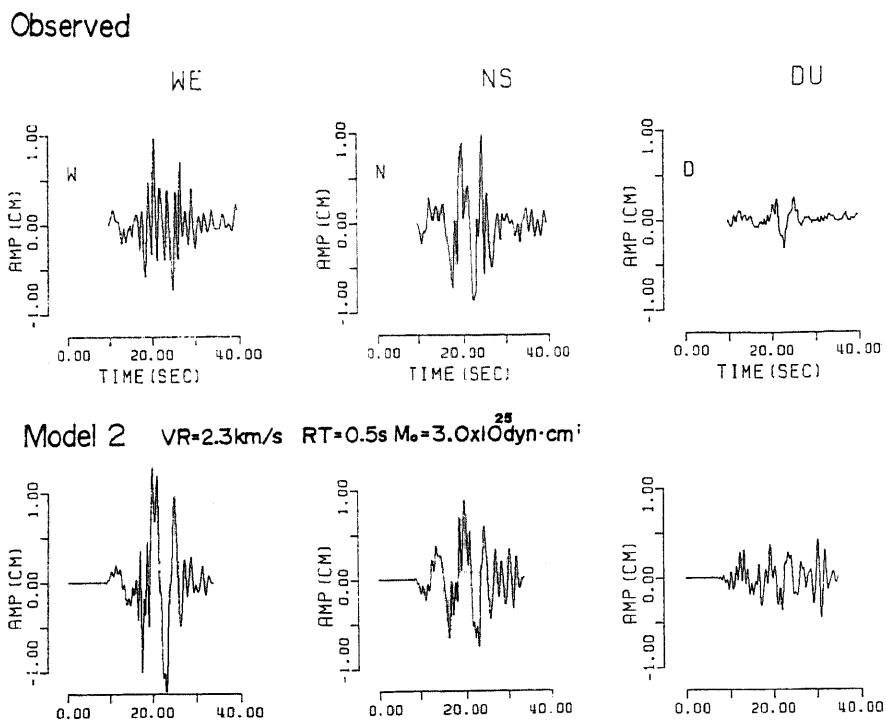

Fig. 9. Strong-motion records from the central Gifu earthquake of September 9, 1969 (M=6.6) at the GIF station, and the corresponding synthetic seismograms computed for Model 2. Rupture velocity VR, rise time RT and seismic moment M_0 are assumed to be 2.3 km/s, 0.5 s and 3.0×10^{25} dyn·cm, respectively.

again that this portion is surface waves amplified by the surficial layers. It has thus been demonstrated that the theoretical synthesis from the Green's functions could be effectively used for predicting ground motions with periods down to about 2–3 s if the surface structure is correctly estimated. However, the vertical component record does not have the reverberations that appear 20 s later in the synthetic seismograms for Model 2, and may be better modeled by Model 1. This may suggest that the actual velocity gradient in the surficial layer is not as sharp as assumed in Model 2.

It should also be mentioned that short-period waves with periods of 1–2 s, which appear 10–20 s after the onset particularly on the E-W component, cannot be simulated by the improved model (Model 2) or even by variations of it within a reasonable range. These unexplained phases might be attributable to the faulting process of the main shock, and should be investigated in more detail.

5. *Results from Semi-Empirical Synthesis Using Aftershock Records*

In this section, some of the results obtained from the semi-empirical analysis

(IMAGAWA and MIKUMO, 1982) are presented, and compared with those from the theoretical synthesis. Since the magnitude of the aftershocks studied here ranges from 4.3 to 4.8, their source area is estimated to be of the order of 1.4 km × 0.7 km to 2.5 km × 1.25 km, if we refer to the empirical relations (13) and (14). In the numerical calculations that follow, we divide the main shock fault plane into 100 segments with an elementary size of 2 km × 1 km, which is approximately the average dimension for these shocks. This implies that the records of 100 aftershocks well located on each of the segments would be required as empirical Green's functions to completely synthesize the main shock records. Since aftershocks with proper sizes are not uniformly distributed over the fault plane, we use four aftershock records to represent approximately the ground motions from the fault segments, by assigning the phase delay time appropriate to each of the segments. Several other shocks are located close to the four shocks used in this study. Their records show very similar waveforms to that of the nearest shock, but remarkably different features for other shocks at somewhat more remote locations. For this reason, we have selected the four aftershocks Nos. 1–4 with appreciably different waveforms that occurred at different locations along the presumed fault, as shown in Fig. 2. We regard these waveforms as representative Green's functions. As in the theoretical synthesis, we assume a radial propagation of the fault rupture, and various rupture velocities ranging between 2.1–3.0 km/s, and rise times 0.2–2.0 s for the main shock and 0.2–0.6 s for the aftershocks, respectively.

Some examples of the results from the semi-empirical synthesis, which are based on Eq. (12), are shown in Figs. 10 and 11. Figure 10 shows the synthetic seismograms calculated for three assumed rupture velocities, 2.1, 2.3, and 2.5 km/s, with a fixed combination of the rise times of 0.2 and 0.5 s, in comparison with the strong-motion records. Figure 11 shows the synthetic seismograms for these different combinations of the rise times with a fixed rupture velocity of 2.3 km/s. In both cases, the ratio of the final displacements between the main shock and aftershocks is assumed to follow the scaling relation (13). As may be expected, we see from these synthetic seismograms that the amplitude increases as the rupture velocity increases and as the rise time of the main shock becomes shorter. The general features of the synthetics given in Figs. 10 and 11, particularly of long-period component waves with periods 5–7 s, appear to be able to account for those of the strong-motion records. The lowest traces in Fig. 11, however, lose short-period content and do not seem consistent with characteristic features of the records, suggesting that the actual rise time of the main shock may not be longer than 1 s. Closer examination of the empirically synthesized seismograms shows that none of the traces for the E-W component are able to explain the short-period waves seen in the record which appear 8 to 15 s after the onset. Also, the third high peak at 15–17 s and its successive short-period wave train on the N-S component record is not modeled by the synthetics.

For the sake of comparison, the results from using only one aftershock, No.

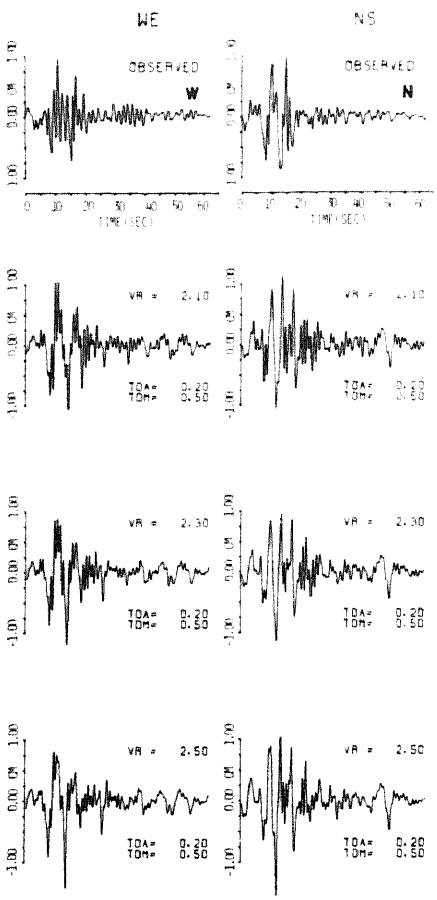

Fig. 10. Strong-motion records of the main shock at the GIF station and the corresponding synthetic seismograms obtained from four aftershock records, for three different rupture velocities and fixed rise times.

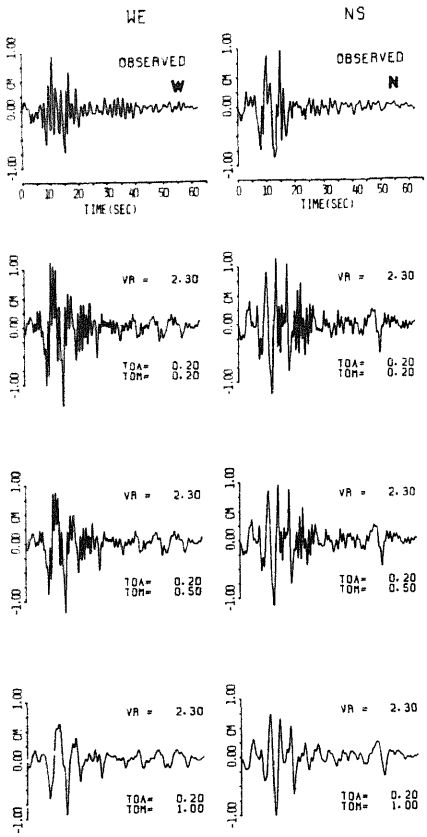

Fig. 11. Strong-motion records of the main shock at the GIF station and the corresponding synthetic seismograms obtained from four aftershock records, for three different combinations of rise times and a fixed rupture velocity.

2, instead of all four shocks, are shown in Fig. 12, where we assumed that its record can be regarded as an approximate Green's function for all fault segments. This figure shows that the long-period waves on two components of the strong-motion records may still be reproduced to some extent by this simplest synthesis. It should be mentioned, however, that the first 10 s of the synthetics lacks short-period components superposed on the long-period waves, and that the peak amplitude ratios between several peaks in the long-period waves are not consistent with those of the records. It is clear from the above results that the semi-empirical synthesis

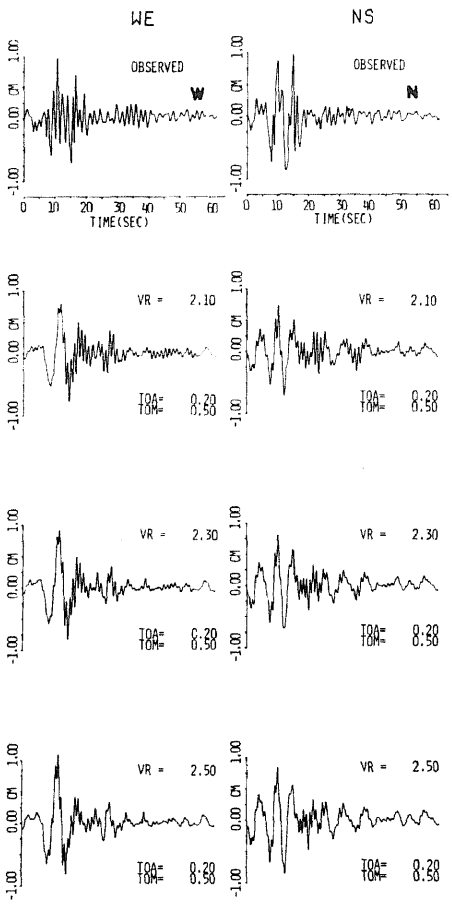

Fig. 12. Strong-motion records of the main shock at the GIF station and the corresponding synthetic seismograms obtained from aftershock record No. 2, for three different rupture velocities with fixed rise times.

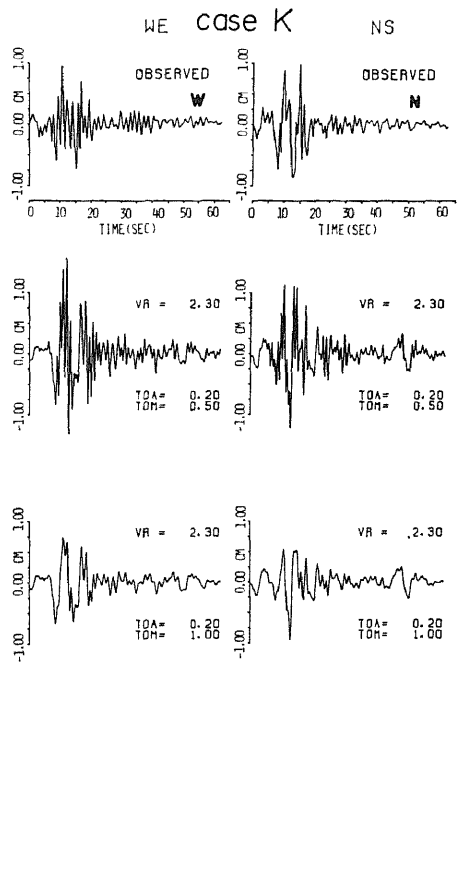

Fig. 13. Synthetic seismograms calculated from a stochastic fault model with variable rupture velocities, incorporating the Green's functions obtained from aftershock records, and the strong-motion records.

using four aftershocks provides better agreement with the data than using only one aftershock. This result may naturally be accepted in view of a reasonable coverage of the four shocks over the fault.

6. *Discussion and Concluding Remarks*

6.1 *Comparison between the results from the theoretical and semi-empirical analyses*

One of the purposes of the present study was to examine the validity of using

the observed seismograms of minor events as empirical Green's functions. As we have shown in Fig. 7, some aftershock records may well be regarded as Green's functions for a point source located at one particular fault segment. This is not always the case, however. In some cases, the aftershock records might be affected by a complicated rupture process, if the event had an appreciable source dimension as in the case of aftershock No. 2. Also, the aftershock may have a radiation pattern which is considerably different from that of the main shock. It should also be pointed out that Green's functions change their waveforms to a considerable extent with the source depth, particularly in a complex crustal structure. This implies that an observed record from a minor event, even if it does not involve the above radiation effects, should only be regarded as representing a Green's function for its focal depth. It is, therefore, extremely important to use the records of minor events that are as well distributed at different depths and horizontal locations over the fault plane as possible. Also, it is important to compare them with the corresponding theoretical Green's functions, in order to investigate closely the fault rupture process of the main shock, although the use of only a few minor shocks has given good results in predicting strong motions in some cases under favorable conditions (e.g., IRIKURA, 1983).

In theoretical synthesis, on the other hand, there are also some problems to be mentioned. The crustal structures, particularly of detailed surficial structures which can seriously effect the recorded waveforms, are not always known to a sufficient degree. As shown for Model 2 in Figs. 6 and 7, low-velocity surficial layers generate large-amplitude converted body waves and surface waves. Incorrect estimates for the surficial structure would lead to unrealistic waveforms. Besides that, various current methods of calculating analytically Green's functions or the response of the medium can only be applied to horizontally layered structure with stepwise or smoothly increasing velocities. Recent seismic studies using inversion techniques have revealed the existence of lateral heterogeneities or three-dimensional structures within the shallow crust in tectonically active regions. If small-scale lateral heterogeneities including topographical site effects exist around the area between the source and receiver, there would be some variations of the seismic waveforms. In the theoretical calculations, attenuative properties have not been taken into account. In the above sense, theoretical calculations may not always be complete to generate Green's functions for realistic structures.

The synthetic seismograms obtained from the theoretical and semi-empirical methods are compared here with the actual strong-motion records. As has been discussed in the preceding section, the recorded waveforms, particularly of long-period body waves and the first portion of surface waves, can be satisfactorily modeled by the theoretical synthesis with a realistic structure, and also, to some extent, by the semi-empirical synthesis with reasonable rupture velocities and rise times. The best agreement between the observed and synthesized waveforms has been obtained for long-period components with periods 5–7 s. The most obvious discrepancy is that the short-period waves with periods 1.5–2.5 s, which arrive

8–15 s after the onset of the E-W component, cannot be well simulated by either of the two different syntheses. This suggests that the discrepancy may not be due to errors such as poor precision in digitization of the observed records or their inadequate representation of the Green's functions.

6.2 A possible model for generating high-frequency waves

A likely explanation for the short-period waves seen in the strong motion records may be a complex faulting process during the main shock. It has been suggested from studies on dynamic rupture process (e.g., MIKUMO and MIYATAKE, 1978; MIYATAKE, 1980) that a strongly heterogeneous distribution of the frictional strengths on the fault will yield stick-slip-like phenomena and incoherent rupture propagation with appreciably variable velocities, which could radiated high frequency seismic waves. Incoherent rupture velocities, non-uniform slip displacements, and episodic source time functions could in principle be derived by using an inversion technique on the seismograms obtained in the near-field, if a number of stations were well distributed around the source area. Since, in the present case, strong-motion records at only a few nearby stations are available, it is practically impossible to do this type of analysis.

On the other hand, a stochastic fault model with non-uniform distributions of displacements, slip angles, rupture velocities, and rise times has been presented (MIKUMO, 1976) to explain a complex faulting process on the basis of a kinematic dislocation model (MARUYAMA, 1963) in an infinite homogeneous medium. In this model, these fault parameters are distributed independently in a normal random fashion with variable standard deviations about their mean values on each fault segment, although these non-uniformities should be closely related to each other from the viewpoint of the dynamic rupture process subjected to the shear stress. From these results (MIKUMO, 1976) and some other studies (MADARIAGA, 1977; BOORE and JOYNER, 1978; IMAGAWA and MIKUMO, 1982; CAMPILLO, 1983), it has been found that the most effective fault parameter to generate high-frequency waves is the rapid variation of the rupture velocity. The effect is strongly enhanced, preserving long-period components, if the rupture accelerates or decelerates over comparatively large-scale fault segments.

Seismic waveforms from the above stochastic model have been calculated for many different cases. The fault plane in this case has been divided into fan-shaped segments with a dimension $\Delta r \times \Delta \varphi$, where Δr and $\Delta \varphi$ are the unit length and azimuthal breadth of the segments, respectively. We assumed that the rupture propagates at different velocities with an average velocity v and a covariance σ_v over each of the segments. An example (Case K) of the synthetic seismograms thus calculated is shown in Fig. 13, which incorporate the empirical Green's functions derived from aftershock records and the incoherent rupture propagation with $v=2.3$ km/s, $\sigma_v=0.5$ km/s, $\Delta r=2$ km, and $\Delta \varphi=30°$ (IMAGAWA and MIKUMO, 1982). Since there could be a number of stochastic spatial distributions of the rupture velocities with the above specifying parameters, it would not be very sig-

nificant to compare the synthetics closely in the time domain with the corresponding strong-motion records. Nevertheless, it may be noticed that this type of incoherent rupture propagation could generate short-period waves. The unexplained short-period phases in the data might be accounted for by this type of incoherent propagation of the fault rupture. This is, of course, one of several possible explanations.

Further sophisticated analysis of the dynamic rupture process undoubtedly requires more detailed information on the crustal structure around the source and recording stations.

We wish to thank Dr. Kojiro Irikura, DPRI, Prof. Ikuei Muramatu, Gifu University, and Dr. Takashi Miyatake, ERI, the University of Tokyo, for their discussion and comments on the semi-empirical analysis. Our thanks are also due Drs. David G. Harkrider and Donald V. Helmberger, Seismological Laboratory, California Institute of Technology, for providing us an original computer code for the DWFE method written by A. Olson. We thank anonymous reviewers for suggestions for the improvement of the original manuscript.

REFERENCES

AKI, K., Seismic displacements near a fault, *J. Geophys. Res.*, **73**, 5359–5376, 1968.

AKI, K. and P. G. RICHARDS, *Quantitative Seismology: Theory and Methods*, Vol. 2, 932 pp., W. H. Freeman, San Francisco, California, 1980.

ALEKSEEV, A. S. and B. G. MIKHAILENKO, Solution of dynamic problems of elastic wave propagation in inhomogeneous media by a combination of partial separation of variables and finite difference method, *J. Geophys.*, **48**, 161–172, 1980.

BOORE, D. M. and W. B. JOYNER, The influence of rupture incoherence on seismic directivity, *Bull. Seismol. Soc. Am.*, **68**, 283–300, 1978.

BOUCHON, M., Predictability of ground displacement and velocity near an earthquake fault. An example: The Parkfield earthquake of 1966, *J. Geophys. Res.*, **84**, 6149–6156, 1979.

BOUCHON, M., The rupture mechanism of the Coyote Lake earthquake of August 6, 1979, inferred from near-field data, presented at the USGS-NRC workshop on strong motion, Lake Tahoe, October, 1981.

BURRIDGE, R. and L. KNOPOFF, Body force equivalents for seismic dislocations, *Bull. Seismol. Soc. Am.*, **54**, 1874–1888, 1964.

CAMPILLO, M., Numerical evaluation of near-field, high-frequency radiation from quasi-dynamic circular faults, *Bull. Seismol. Soc. Am.*, **73**, 723–734, 1983.

FUCHS, K. and G. MÜLLER, Computation of synthetic seismograms with reflectivity method and comparison with observations, *Geophys. J. R. Astron. Soc.*, **23**, 417–433, 1971.

HADLEY, D. M. and D. V. HELMBERGER, Simulation of strong ground motion, *Bull. Seismol. Soc. Am.*, **70**, 617–630, 1980.

HARTZELL, S. H., Earthquake aftershocks as Green's Functions, *Geophys. Res. Lett.*, **5**, 1–4, 1978.

HASKELL, N., Elastic displacement in the near-field of a propagating fault, *Bull. Seismol. Soc. Am.*, **59**, 869–908, 1969.

HEATON, T. H. and D. V. HELMBERGER, A study of the strong ground motion of the Borrego Mountain, California, earthquake, *Bull. Seismol. Soc. Am.*, **67**, 315–330, 1977.

HEATON, T. H. and D. V. HELMBERGER, Predictability of strong ground motion in the Imperial Valley; Modeling the M 4.9, November 4, 1976 Brawley earthquake, *Bull. Seismol. Soc. Am.*, **68**, 31–48, 1978.

HELMBERGER, D. V., The crust-mantle transition in the Bering Sea, *Bull. Seismol. Soc. Am.*, **58**, 179–214, 1968.

HELMBERGER, D. V. and S. D. MALONE, Modeling local earthquakes as shear dislocations in a layered half-space, *J. Geophys. Res.*, **80**, 4881–4888, 1975.

HERRMANN, R. B., Research study of earthquake generated SH waves in the near-field and near-regional field. Final report, contact DACW39-76-C-0058 Waterways Experiment Station, Vicksburg, Miss, 1977.

HERRMANN, R. B. and O. W. NUTTLI, Ground-motion modeling at regional distances for earthquakes in a continental interior. I. Theory and Observations, *Earthq. Eng. Struct. Dyn.*, **4**, 49–58, 1975a.

HERRMANN, R. B. and O. W. NUTTLI, Ground-motion modeling at regional distances for earthquakes in a continental interior. II. Effects of focal depth, *Earthq. Eng. Struct. Dyn.*, **4**, 59–72, 1975b.

HRON, F. and B. G. MIKHAILENKO, Numerical modelling of non-geometrical effects by the Alekseev-Mikhailenko method, *Bull. Seismol. Soc. Am.*, **71**, 1011–1029, 1981.

IMAGAWA, K. and T. MIKUMO, Near-field seismic waveforms from major earthquakes and a consideration on the rupture process on the fault, *Zisin (J. Seismol. Soc. Jpn.), Ser. 2*, **35**, 575–590, 1982 (in Japanese).

IRIKURA, K., Semi-empirical estimation of strong ground motions during large earthquakes, *Bull. Disast. Prev. Res. Inst., Kyoto Univ.*, **33**, 63–104, 1983.

IRIKURA, K. and I. MURAMATU, Synthesis of strong ground motions from large earthquakes using observed seismograms of small events, *Proceedings Third International Earthq. Microzonation Conf.*, Seattle, Vol. 1, 447–458, 1982.

KANAMORI, H., A semi-empirical approach to prediction of long-period ground motions from great earthquakes, *Bull. Seismol. Soc. Am.*, **69**, 1645–1670, 1979.

KANAMORI, H. and D. L. ANDERSON, Theoretical basis of some empirical relations in seismology, *Bull. Seismol. Soc. Am.*, **65**, 1073–1095, 1975.

KAWASAKI, I., The near-field Love wave by the exact ray method, *J. Phys. Earth*, **26**, 211–237, 1978.

KAWASAKI, I., Y. SUZUKI, and R. SATO, Seismic waves due to a shear fault in a semi-infinite medium. Part 1. Point source, *J. Phys. Earth*, **21**, 251–284, 1973.

KAWASAKI, I., Y. SUZUKI, and R. SATO, Seismic waves due to a shear fault in a semi-infinite medium. Part 2. Moving source, *J. Phys. Earth*, **23**, 43–61, 1975.

KENNETT, B. L. N., Reflections, rays and reverberations, *Bull. Seismol. Soc. Am.*, **64**, 1685–1696, 1974.

KENNETT, B. L. N. and N. J. KERRY, Seismic waves in a stratified half space, *Geophys. J. R. Astron. Soc.*, **57**, 557–583, 1979.

MADARIAGA, R., High-frequency radiation from crack (stress drop) models of earthquake faulting, *Geophys. J. R. Astron. Soc.*, **51**, 625–651, 1977.

MARUYAMA, T., On the force equivalents of dynamical elastic dislocations with reference to the earthquake mechanism, *Bull. Earthq. Res. Inst.*, **41**, 467–486, 1963.

MIKUMO, T., Faulting mechanism of the Gifu earthquake of September 9, 1969, and some related problems, *J. Phys. Earth*, **21**, 191–212, 1973.

MIKUMO, T., Theoretical estimates of seismic ground motions near a fault. Part 3. Possibility of generation of high-frequency seismic waves, Project Rep. 50-I-2-(1), *Build. Res. Inst.*, 191–212, 1976 (in Japanese).

MIKUMO, T., Prediction of strong motions near a fault during a major earthquake from the synthesis of minor shock records, Rep. Natural Disaster No. A-56-3, Science Research Fund, the Ministry of Education, Science and Culture of Japan, 25–30, 1981 (in Japanese).

MIKUMO, T. and T. MIYATAKE, Dynamical rupture processes on a three-dimensional fault with

non-uniform frictions, and near-field seismic waves, *Geophys. J. R. Astron. Soc.*, **54**, 417–438, 1978.

MIYATAKE, T., Numerical simulations of earthquake source process by a three-dimensional crack model, *J. Phys. Earth*, **28**, 565–616, 1980.

OLSON, A. H., Forward simulation and linear inversion of earthquake ground motions, Ph. D. thesis, University of California, San Diego, 1982.

SATO, R., Long-period surface velocities and accelerations due to a dislocation source model in a medium with superficial multi-layers. Part 1, *J. Phys. Earth*, **25**, 43–68, 1977.

SATO, R., Long-period surface velocities and accelerations due to a dislocation source model in a medium with superficial multi-layers. Part 2, *J. Phys. Earth*, **26**, 17–37, 1978.

SATO, R. and N. HIRATA, One method to compute theoretical seismograms in a layered medium, *J. Phys. Earth*, **28**, 145–168, 1980.

SWANGER, H. J. and D. M. BOORE, Simulation of strong-motion displacements using surface-wave modal superposition, *Bull. Seismol. Soc. Am.*, **68**, 907–922, 1978.

UKAWA, M. and Y. FUKAO, Poisson's ratios of the upper and lower crust and the sub-Moho mantle beneath central Honshu, Japan, *Tectonophysics*, **77**, 233–256, 1982.

WIGGINS, R. A., J. SWEET, and G. A. FRAZIER, The Parkfield earthquake of 1966. A study of the dislocation parameters based on a complete modeling of elastic wave propagation, *Trans. Am. Geophys. Union*, **58**, 1193, 1977.